Rapid 3-D Magnetic Integral Field Computation of Current-Carrying Finite Arc Segments with Rectangular Cross-Section

Frederic Maurer[1], Basile Kawkabani[1], *Senior Member, IEEE*, and Jonas Kristiansen Nøland[2], *Member, IEEE*

[1] Ecole Polytechnique Federale de Lausanne, Station 17, CH-1015 Lausanne, Switzerland

[2]Department of Electric Power Engineering, Norwegian University of Science and Technology, Trondheim, Norway

The computation of three-dimensional (3-D) magnetic fields is a demanding task in the analysis of electrical machines and other electromagnetic devices. In this context, integral field calculation provides a smooth solution, high precision and resolution, "on-demand"-calculation, and an origin-based formulation of the magnetic field and the magnetic vector potential. However, conventional elliptic methods lead to huge parallelizable computing efforts and significant errors. In this paper, a 3-D generic current-carrying arc segment with rectangular cross-section is studied. A new analytic formulation is proposed to speed up the computation of magnetic fields and reduce the error by more than three orders of magnitude. In addition, the proposed magnetic vector potential expression has similar accuracy as numerical integration. In fact, a significant reduction of the error level has been showcased clearly with respect to existing approaches. The present work is promising for improving the design methodology and optimization of large superconducting dipole magnets or arched end-winding geometries of large electrical machines.

Index Terms—**Analytical formulation, arch segments, 3-D magnetic fields, integral calculation, end-winding, supra-conductive coils.**

I. NOMENCLATURE

The nomenclature this paper is adopted from common terminology [7], where

- φ_1, φ_2, $\phi = \varphi' - \varphi$, α (defined in eq. (14)) angles [rad],
- r_1, r_2, r, r' radial distances [m],
- $\gamma = z' - z$, z_1, z_2, z, z' axial distances [m],
- $\vec{H}$ (magnetic field) is the $\vec{H}$-field in this paper [A/m],
- $\vec{B}$ (magnetic flux density) is $\vec{B}$-field in this paper [T],
- $\vec{A}$ (magnetic vector potential) is the $\vec{A}$-field in this paper [Wb/m],

Fig. 1 defines the quantities and subscripts geometrically. The integration domain is not mentioned explicitly and ranges from $r = r_1$ to $r = r_2$ for the integration along the radial component, from $\varphi = \varphi_1$ to $\varphi = \varphi_2$ for the integration along the tangential component and from $z = z_1$ and $z = z_2$ for the integration along the axial component.

The cylindrical coordinates z, r and φ are the global coordinate system, whereas z', r' and φ' are used as the source coordinate system when deriving the integral equations.

II. INTRODUCTION

THE calculation of complex three-dimensional (3-D) $\vec{H}$-fields from current-carrying conductors are conventionally done in the finite element (FE) environment. Arced current-carrying bodies appear in 3-D geometries such as coils of electromagnetic devices, winding overhangs (end-windings) of electrical machines or supra-conductive coils, in particular.

Recently, analytic calculations experienced a come-back in several publications related to superconducting shim coil [1] or related to mutual inductance and force calculation for circular coils with rectangular cross-section [2]–[4]. Mostly, the integral method is used in combination with geometry optimisation problems in coil and winding design areas. Moreover, this method can also serve as a pre-calculation of the electric vector potential T0 for magneto-static (also called T0-ψ) or -dynamic (also called T0-T-ψ) FE problems, for which ψ is the reduced potential and T the electric vector potential associated to eddy-currents [5]. Moreover, in the case of large synchronous generators (spanning from a stator bore diameter of 2.0 to 18.0 m), the simulation model can cover up to half of the whole machine geometry. As a result, an unmanageable mesh size is needed. In comparison, a 700 MB RAM memory is needed for a complete overhang model of a 12-pole, 4.3 m bore diameter electrical machine modelled using the integral method.

Many numerical-analytic formulations of 3-D $\vec{H}$-fields were proposed in the time span from approx. 70's to 90's. However, over time, they were inevitably substituted by the FE methodology. The main reason lies in their main drawbacks, i.e., they need of numerical evaluation of elliptic integrals of the first, second and third kind, which were, in fact, very time consuming until a breakthrough made in 2009 by Fukushima [6]. Moreover, floating-point operations are intensive and not easily parallelizable for a single-point computation. On the contrary, the FE methods can easily be parallelized and could also take full advantage of the increasing computing power. As a result, integral formulation reduced their applicability over time, which explains the fact that most papers related to
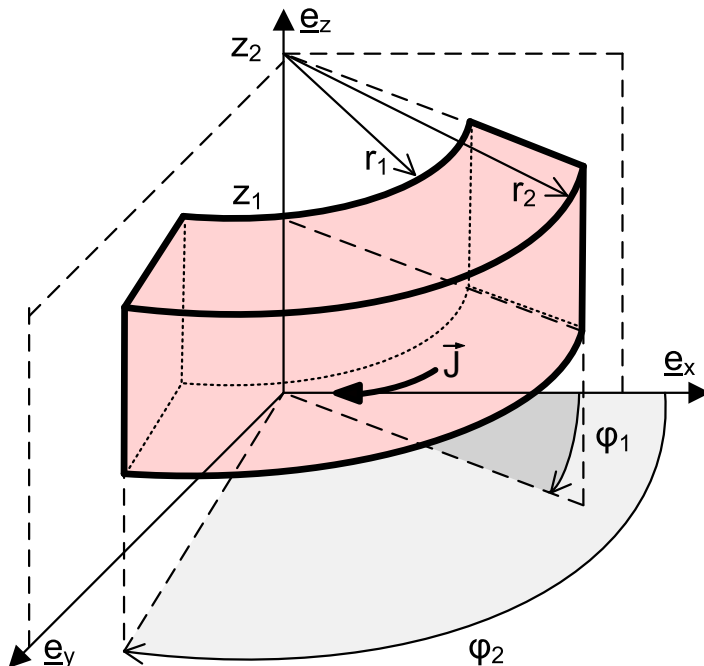
Fig. 1: Schematic representation of the generalized arch segment of a current path with rectangular cross-section.

analytic field calculation are more than 35 years old. In fact, it is nearly a forgotten chapter of magnetic field analysis. As a result, the hidden potential for significant improvements has been historically overlooked.

In a series of six publications [7] - [12], Urankar presents analytic formulations to obtain the $\vec{H}$-field and $\vec{A}$-field for straight and arched conductors with various cross-sections. In [13] and [14], the authors presents analytic formulae for the $\vec{H}$-field of a closed arched current-carrying conductor, which are identical up to a sign-function to the particular case presented in [7]. Unfortunately, these publications lack validation of their formulations. Later, the analytic formulations for the $\vec{H}$-field were compared with the results of a volume integral method (VIM) [15]. The equations generates values that slightly differs from the ones presented in [7], and with significant differences to the values obtained by the VIM. This may be a reason of their rather low use in the scientific community. In fact, no publications reported any validation of the $\vec{A}$-field formulas presented in [7]. The $\vec{A}$-field has a couple of practical applications. In the context of coil design (supra-conductive or not), the $\vec{A}$-field can be used to obtain the inductance in a more straightforward way than using the magnetic energy and a volume integral. In the context of time-evolutive field simulation, the $\vec{A}$-field is a key variable to obtain the induced voltage from which, one can deduce, e.g., the circulating current in the Roebel bar of an electrical machine. In addition, it can be used to calculate 3-D eddy currents [16], or more generally

speaking, couple an analytical 3-D winding overhang (or edge-field) model with a classical 2-D FE model, to make the best use of the advantages of both methods.

In order to achieve low computational costs in the calculation, one have to rely on precise and fast algorithms to evaluate them. Urankar identified this issue and proposed in [17] and [18] solutions to increase the computational speed. In addition, Fukushima made a breakthrough in the calculation of elliptic integral proposed in a series of papers [6], [19]–[24] where novel approaches and algorithms reduced the computation time by at least one order of magnitude compared to former methods developed by Bulirsch or Carlson ([6], [19]–[24] uses their foundations). Incorporating this achievement, the computation time is not anymore the limiting factor to the practical implementation of analytic formulations. However, significant numerical discrepancies as shown in [15] are still an issue, which are the main objective of this paper.

In this paper, a generic problem is showcase to represents a wide range of applications, as described in from the beginning of this section. In the present work, improved analytic formulae for the $\vec{H}$-field and $\vec{A}$-field are derived starting from the expressions presented in [7]. The analytic expressions for the $\vec{H}$-field and the $\vec{A}$-field are inherently precise. In addition, they also provide the $\vec{H}$-fields' contribution of each element of a complex geometry. From [7], this work develops improved expressions for the $\vec{B}$-field and the $\vec{A}$-field for an arched current-carrying conductor with rectangular cross-section (refer to Fig. 1) as the analytic formulas developed in [7] appears to have some integration errors (refer to the errors presented in Table IV, Section V). To correct them, a novel analytic development of the complete set of equations has been carried out. These novel expressions are validated using FE simulations and assessed against the work of Fontana [15] as a benchmark. The novel expressions for the $\vec{A}$-field are compared with a numerical integration performed with the MATLAB numerical environment. Practical implementation of these improved formulae make an extensive use of the elliptic integral calculation algorithms developed in [6] to [24], which reduces the calculation time by at least one order of magnitude ([6] - [24]).

The paper is organized as follows. In Section III, the basic integrals for the generic problem is presented. Further, the novel expressions are derived in Section IV. In Section V, the expressions are evaluated in a generalized case study. Finally, Section VI concludes the paper and offers a view on future perspectives and open issues.

III. BASIC INTEGRALS

Fig. 1 shows a schematic representation of an arched current-carrying conductor with rectangular cross-section where the nomenclature presented in Section I is used. The integral equations for the vector potential, $\vec{A}(\vec{r})$, and the magnetic flux density, $\vec{B}(\vec{r})$, are obtained from the law of Biot-

Savart applied to a known constant current density $\vec{J} = j\vec{e}_{\phi'}$ over a rectangular cross-section. They are given by

$$\vec{A}(\vec{r}) = \frac{\mu_0 j}{4\pi} \int_{\varphi} \int_r \int_z \frac{r' \vec{e}_{\phi'}}{|\vec{r} - \vec{r}'|} dz' dr' d\phi \quad (1)$$

$$\vec{B}(\vec{r}) = \frac{\mu_0 j}{4\pi} \int_{\varphi} \int_r \int_z \frac{r' \vec{e}_{\phi'} \times (\vec{r} - \vec{r}')}{|\vec{r} - \vec{r}'|^3} dz' dr' d\phi \quad (2)$$

where j is the known uniform current density expressed in ampere per square meter, $\vec{e}_{\phi'} = -\sin(\phi)\vec{e}_r + \cos(\phi)\vec{e}_{\varphi}$ is the unit vector in tangential direction of the local (or source) cylindrical coordinate system (r',ϕ',z'), the global one being (r,φ,z) , $\int_{\phi}$ the integral over the tangential coordinate ϕ of the local (or source) cylindrical coordinate system, $\int_r \int_z$ the surface integral over the radial and axial coordinates r' and z' of the local (or source) cylindrical coordinate system, $\vec{r}$ the vector to the point where the potential vector ($\vec{A}$-field) respectively magnetic flux density ($\vec{B}$-field) is calculated, $\vec{r}'$ is a vector pointing to a source point located in the volume to be integrated and defined by $[r_1,r_2] \times [\varphi_1,\varphi_2] \times [z_1,z_2]$ (refer to fig. 1) and μ_0 is the permeability of the vacuum $(4\pi 10^{-7} N/A^2)$. Refer to section I for the definition of the variables used in this article.

The constant current density hypothesis has been assumed as it is a common practice for this kind of problems and is widely used in the literature (refer for example [7]–[10] and [1], [3], [28]–[32]) covering a wide range of applications from integral field calculation, to analytic inductance calculations passing through design optimisation of end-windings or large superconducting coils. The second reason lies in its intrinsic simplicity. The hypothesis can easily model any current density by changing the current passing through each conductor with a rectangular cross-section and by adjusting adequately the cross-section and intrinsic current density of each conductor.

IV. NOVEL ANALYTIC EXPRESSIONS

This section derives the novel analytical formulations proposed in this paper. In the introductory part, general expressions of the $\vec{A}$-field and the $\vec{B}$-field are prepared. The following subsections derives the improved formulations step by step in detail.

Analytic expression has already been formulated with elliptical integrals [7]. In fact, it is possible to obtain a reduced expression without elliptic integrals, i.e., first integrate over the angle ϕ and then over the other variables (r' and z'). In eq. (1), denominator $|\vec{r} - \vec{r}'|$ is replaced by $D(\phi)$, clearly defined by eq. (9). In fact, $D(\phi)$ is also a function of z' and r', but it will not be formulated explicitly to remain consistent with the notation defined in [7]. Using the nomenclature defined in Section I and the framework outlined in eqs. (8) to (13), the analytic derivations are made. Integrating over ϕ (integration

by substitution) then over r' and finally over z', one obtains finally

$$A_r = \frac{\mu_0 j}{4\pi} \int_{\varphi} \int_r \int_z \frac{-r' \sin(\phi)}{D(\phi)} dz' dr' d\phi$$

$$= \frac{\mu_0 j}{\pi} \left[\frac{a}{4r} \left[\gamma D(\phi) + B^2(\phi) \sinh^{-1} \left(\beta_2(\phi) \right) \right] \right.$$

$$+ \frac{1}{12r} \left[a\gamma D(\phi) - a(a^2 - 3b^2) \sinh^{-1} \left(\beta_2(\phi) \right) \right]$$

$$- 4b^3 \tan^{-1} \left(\beta_3(\phi) \right)$$

$$+ \left(2\gamma^3 + 6b^2\gamma \right) \sinh^{-1} \left(\frac{a}{\sqrt{b^2 + \gamma^2}} \right) \right] \Bigg|_{r'=r_1}^{r'=r_2} \Bigg|_{\phi=\varphi_1-\varphi}^{\phi=\varphi_2-\varphi} \Bigg|_{z'=z_1}^{z'=z_2}$$

$$(3)$$

where $a = r' - r\cos(\phi)$, $b = r\sin(\phi)$ and ϕ are spanning over $[\varphi_1 - \varphi, \varphi_2 - \varphi]$. Note that $-\varphi$ will be left out in the following equations to formulate "lighter" equations, where it will be understood as implicit. The formula derived in eq. (3) is verified using an analytic integration software (such as Mathematica) and will therefore be assumed as a premise in the following sections.

The formulation of A_{φ} will be expressed hereafter without the factor $\mu_0 j/4\pi$ (compressed formulation). In the derivation of A_{φ}, the integration over the variables r' and z' is straightforward and the obtained expression has already been reported [7]. and they are recalled hereafter. The expression for the tangential component of the $\vec{A}$-field presented [7] contained errors and it was not possible to correct them. On the contrary, as stated in [7], there is no need for a double integration by parts. The novel expression can be derived using a single integration by parts obtaining the novel expression for the $\vec{A}$-field. Recalling eq. (3.b) of [7] leads to

$$A_{\varphi} = \frac{1}{2} \int_{\varphi_1}^{\varphi_2} d\phi \Big(\gamma D(\phi) + 2\gamma r \cos(\phi) \sinh^{-1} \beta_1(\phi)$$

$$+ \left(r'^2 - r^2 \cos(2\phi) \right) \sinh^{-1} \beta_2(\phi)$$

$$- r^2 \sin(2\phi) \tan^{-1} \beta_3(\phi) \Big) \cos(\phi). \quad (4)$$

The formulation of the $\vec{B}$-field will also be normalized hereafter by $\mu_0 j/4\pi$. In this context, the same errors in the formulas are considered and a single integration by parts can be made. The radial component can also be computed without any elliptic integrals. The proposed novel expression can be derived using a single integration by parts. It follows accordingly that the

expression to be integrated yields

$$H_r = \int_{\varphi_1}^{\varphi_2} d\phi \Big[\cos(\phi) D(\phi) + r \cos(\phi)^2 \sinh^{-1} \beta_1(\phi) \Big] \quad (5)$$

$$H_\varphi = \int_{\varphi_1}^{\varphi_2} d\phi \int_{r_1}^{r_2} dr' \int_{z_1}^{z_2} dz' \ \frac{-\gamma r' \sin(\phi)}{D(\phi)^3} \quad (6)$$

$$H_z = \int_{\varphi_1}^{\varphi_2} d\phi \Big[\gamma \sinh^{-1} \beta_1(\phi) - r \cos(\phi) \sinh^{-1} \beta_2(\phi) \quad (7)$$
$$- r \sin(\phi) \tan^{-1} \beta_3(\phi) \Big]$$

where the nomenclature and variables (namely $B, D, G, \beta_1, \beta_2$ and β_3) defined in [7] and the following variables have been partially utilized in Section I.

$$B^2(\phi) = r^2 + r'^2 - 2rr' \cos(\phi) \quad (8)$$
$$D^2(\phi) = \gamma^2 + B^2(\phi) \quad (9)$$
$$G^2(\phi) = \gamma^2 + r^2 \sin(\phi) \quad (10)$$
$$\beta_1(\phi) = (r' - r \cos(\phi))/G(\phi) \quad (11)$$
$$\beta_2(\phi) = \gamma/B(\phi) \quad (12)$$
$$\beta_3(\phi) = \gamma(r' - r \cos(\phi))/[r \sin(\phi) D(\phi)] \quad (13)$$

where γ have been defined in Section I. The integrals transformed along the tangential coordinate into elliptic integrals using the same angle transformation as in [7], yields

$$\phi = \pi - 2\alpha. \quad (14)$$

The elliptic integral coefficients are given by

$$k^2 = \frac{4rr'}{\gamma^2 + (r + r')^2} \quad (15)$$
$$a^2 = \gamma^2 + (r + r')^2 \quad (16)$$
$$n^2 = \frac{4rr'}{(r + r')^2}. \quad (17)$$

Using these constants, the angle transformation will derive the following expressions

$$B^2(\alpha) = r^2 + r'^2 - 2rr' \cos(\phi) \quad (18)$$
$$= (r + r')^2(1 - n^2 \sin(\alpha)^2)$$
$$D^2(\alpha) = \gamma^2 + B^2(\phi) = a^2(1 - k^2 \sin(\alpha)^2). \quad (19)$$

In dealing with $G(\phi)$, the expression expressed in terms of $1/G(\alpha)^2$ yields

$$G^{-2}(\alpha) = \frac{1}{2\sqrt{\gamma^2 + r^2}} \Big(\frac{1}{(\sqrt{\gamma^2 + r^2} - r)(1 - n_1^2 \sin(\alpha)^2)}$$
$$(20)$$
$$+ \frac{1}{(\sqrt{\gamma^2 + r^2} + r)(1 - n_2^2 \sin(\alpha)^2)} \Big)$$

with

$$n_1^2 = \frac{2r}{r - \sqrt{\gamma^2 + r^2}} \quad (21)$$
$$n_2^2 = \frac{2r}{r + \sqrt{\gamma^2 + r^2}}. \quad (22)$$

Finally, integration over the angle ϕ achieves the improved analytic expressions.

It has been decided to integrate the expressions only once per part, which is the main difference with the expressions presented in [7]. To obtain compact expressions, one uses extensively the formulas for the *sine* respectively *cosine* of the double of the argument. For A_r and H_φ, the improved solutions does not contain any elliptic integrals due to a first integration over ϕ followed by integration over r' and then z'. To obtain expressions without any elliptic integrals, one have to to use integration by substitution, substituting $-2rr' \cos(\phi)$ by x.

In the following subsections, improved formulations of the angular $\vec{A}$-field (A_φ), the angular $\vec{H}$-field (H_φ), the radial $\vec{H}$-field (H_r) and the axial $\vec{H}$-field (H_z) will be derived. Finally, the numerical computation algorithms will be summarised.

A. Improved formulation of the angular vector potential A_φ

Eq. (4) is divided into four integrals, which will be integrated using a single integration by parts, yielding

$$I_1 = \frac{1}{2} \int_{\varphi_1}^{\varphi_2} d\phi \ \ \gamma D(\phi) \cos(\phi) \quad (23)$$

$$I_2 = \int_{\varphi_1}^{\varphi_2} d\phi \ \ \gamma r \cos(\phi)^2 \sinh^{-1} \beta_1(\phi) \quad (24)$$

$$I_3 = \frac{1}{2} \int_{\varphi_1}^{\varphi_2} d\phi \ \ \left(r'^2 - r^2 \cos(2\phi) \right) \sinh^{-1} \beta_2(\phi) \cos(\phi)$$
$$(25)$$

$$I_4 = -\frac{1}{2} \int_{\varphi_1}^{\varphi_2} d\phi \ \ r^2 \sin(2\phi) \tan^{-1} \beta_3(\phi)) \cos(\phi), \quad (26)$$

where

$$A_\varphi = I_1 + I_2 + I_3 + I_4. \quad (27)$$

1) Integral I_1 of A_φ

The integral I_1 is transformed into an elliptical integral and solved to obtain

$$I_1 = \frac{1}{2} \int_{\varphi_1}^{\varphi_2} d\phi \ \ \gamma D(\phi) \cos(\phi)$$

$$= \gamma a \int_{\alpha_1}^{\alpha_2} d\alpha \big(1 - 2\sin(\alpha)^2\big) \sqrt{1 - k^2 \sin(\alpha)^2}$$

$$= \gamma a \Big(E(\alpha, k^2) + 2\gamma a \Big(\frac{1}{3} \big(\frac{1}{k^2} - 1 \big) F(\alpha, k^2) $$
$$+ \frac{1}{3} \big(2 - \frac{1}{k^2} \big) E(\alpha, k^2)$$
$$- \frac{1}{3} \sin(\alpha) \cos(\alpha) \sqrt{1 - k^2 \sin(\alpha^2)} \Big) \Big) \Big|_{\alpha = \alpha_1}^{\alpha = \alpha_2} \quad (28)$$

where $F(\alpha, k)$ is the first order elliptic integral and $E(\alpha, k)$ is the second order elliptic integral, k is given by eq. (15) and a is defined in eq. (16).

2) Integral I_2 of A_φ

Applying a similar transformation for the integral I_2 yields

$$
\begin{aligned}
I_2 &= \int_{\varphi_1}^{\varphi_2} d\phi \gamma r \cos(\phi)^2 \sinh^{-1}\left(\beta_1(\phi)\right) \\
&= \frac{1}{2}\gamma r \int_{\varphi_1}^{\varphi_2} d\phi \sinh^{-1}\left(\beta_1(\phi)\right) \\
&\quad + \frac{1}{2}\gamma r \int_{\varphi_1}^{\varphi_2} d\phi \cos(2\phi) \sinh^{-1}\left(\beta_1(\phi)\right) \\
&= I_{2a} + I_{2b}.
\end{aligned}
\tag{29}
$$

The first integral (I_{2a}) will be solved numerically, as no analytic expression can be found for it. For the second part, integration by parts leads to

$$
\begin{aligned}
I_{2b} &= \frac{1}{2}\gamma r \int_{\varphi_1}^{\varphi_2} d\phi \cos(2\phi) \sinh^{-1}\left(\beta_1(\phi)\right) \\
&= \frac{1}{4}\gamma r \sin(2\phi) \sinh^{-1}\left(\beta_1(\phi)\right)\Big|_{\phi=\varphi_1-\varphi}^{\phi=\varphi_2-\varphi} \\
&\quad - \frac{1}{4}\gamma r \int_{\varphi_1}^{\varphi_2} d\phi \sin(2\phi)\Big[\frac{r\sin(\phi)}{D(\phi)} \\
&\quad - r^2 \frac{\cos(\phi)\sin(\phi)r' - r\cos(\phi)^2\sin(\phi)}{G(\phi)D(\phi)}\Big] \\
&= I_{2b1} + I_{2b2}.
\end{aligned}
\tag{30}
$$

To further simplify, I_{2b2} is divided into two parts

$$
\begin{aligned}
I_{2b2,1} &= -\frac{1}{4}\gamma r \int_{\varphi_1}^{\varphi_2} d\phi \quad \sin(2\phi)\frac{r\sin(\phi)}{D(\phi)} \\
&= \frac{1}{a}\gamma r^2 \int_{\alpha_1}^{\alpha_2} d\alpha \quad \frac{\sin(\alpha)^2\cos(\alpha)^2(1-2\sin(\alpha)^2)}{\sqrt{1-k^2\sin(\alpha^2)}} \\
&= \frac{1}{a}\gamma r^2 \int_{\alpha_1}^{\alpha_2} d\alpha \quad \frac{\alpha_0 + \alpha_2\sin(\alpha)^2 + \alpha_4\sin(\alpha)^4}{\sqrt{1-k^2\sin(\alpha^2)}} \\
&\quad + \frac{\alpha_6\sin(\alpha)^6}{\sqrt{1-k^2\sin(\alpha^2)}}
\end{aligned}
\tag{31}
$$

and

$$
\begin{aligned}
I_{2b2,2} &= \frac{1}{4}\gamma r^3 \int_{\varphi_1}^{\varphi_2} d\phi \quad \sin(2\phi)\frac{\cos(\phi)\sin(\phi)r'}{G(\phi)D(\phi)} \\
&\quad - \frac{r\cos(\phi)^2\sin(\phi)}{G(\phi)D(\phi)} \\
&= \frac{1}{2}\gamma r^3 \int_{\varphi_1}^{\varphi_2} d\phi \quad \frac{\cos(\phi)^2\sin(\phi)^2 r' - r\cos(\phi)^3\sin(\phi)^2}{G(\phi)D(\phi)} \\
&= -\frac{1}{2a}\gamma r^3 \int_{\alpha_1}^{\alpha_2} d\alpha \quad \frac{\alpha_0 + \alpha_2\sin(\alpha)^2 + \alpha_4\sin(\alpha)^4}{G(\alpha)\sqrt{1-k^2\sin(\alpha^2)}} \\
&\quad + \frac{\alpha_6\sin(\alpha)^6 + \alpha_8\sin(\alpha)^8 + \alpha_{10}\sin(\alpha)^{10}}{G(\alpha)\sqrt{1-k^2\sin(\alpha^2)}}.
\end{aligned}
\tag{32}
$$

The final results for the integrals of eqs. (31) and (32) can be found using [33].

3) Integral I_3 of A_φ

The third integral will be decomposed in two parts

$$
\begin{aligned}
I_{3b1} &= \frac{1}{2}r'^2 \int_{\varphi_1}^{\varphi_2} d\phi \quad \cos(\phi)\sinh^{-1}\left(\beta_2(\phi)\right) \\
I_{3b2} &= -\frac{1}{2}r^2 \int_{\varphi_1}^{\varphi_2} d\phi \quad \cos(2\phi)\cos(\phi)\sinh^{-1}\left(\beta_2(\phi)\right).
\end{aligned}
\tag{33}
$$

Further, integration by parts yields

$$
\begin{aligned}
I_{3b1} &= \frac{1}{2}r'^2 \int_{\varphi_1}^{\varphi_2} d\phi \quad \cos(\phi)\sinh^{-1}\left(\beta_2(\phi)\right) \\
&= \frac{1}{2}r'^2 \sin(\phi)\sinh^{-1}\left(\beta_2(\phi)\right)\Big|_{\phi=\varphi_1-\varphi}^{\phi=\varphi_2-\varphi} \\
&\quad + \frac{1}{2}r'^3 r \int_{\varphi_1}^{\varphi_2} d\phi \quad \frac{\sin(\phi)^2}{B^2(\phi)D(\phi)}
\end{aligned}
\tag{34}
$$

for I_{3b1}. This integral can be transformed into an elliptic integral

$$
\begin{aligned}
I_{3b1} &= -r'^3 r \int_{\varphi_1}^{\varphi_2} d\alpha \quad \frac{4\sin(\alpha)^2(1-\sin(\alpha)^2)}{B^2(\alpha)D(\alpha)} \\
&= -r'^3 r \int_{\varphi_1}^{\varphi_2} d\alpha \quad \frac{4\sin(\alpha)^2 - 4\sin(\alpha)^4}{B^2(\alpha)D(\alpha)}.
\end{aligned}
\tag{35}
$$

Applying the same methodology for the second integral I_{3b2}, one obtains

$$
\begin{aligned}
I_{3b2} &= -\frac{1}{2}r^2 \int_{\varphi_1}^{\varphi_2} d\phi \quad \cos(2\phi)\cos(\phi)\sinh^{-1}\left(\beta_2(\phi)\right) \\
&= -\frac{1}{2}r^2 \int_{\varphi_1}^{\varphi_2} d\phi \quad (1-2\sin(\phi)^2)\cos(\phi)\sinh^{-1}\left(\beta_2(\phi)\right) \\
&= I_{3b21} + I_{3b22}.
\end{aligned}
\tag{36}
$$

For the first part of the integral (I_{3b21}), please refer to the treatment of integral I_{3b1}. For the second part, integration by parts leads to

$$
\begin{aligned}
I_{3b22} &= r^2 \int_{\varphi_1}^{\varphi_2} d\phi \quad \sin(\phi)^2\cos(\phi)\sinh^{-1}\left(\beta_2(\phi)\right) \\
&= \frac{r^2}{3}\sin(\phi)^3 \sinh^{-1}\left(\beta_2(\phi)\right)\Big|_{\phi=\varphi_1-\varphi}^{\phi=\varphi_2-\varphi} \\
&\quad \underbrace{-\frac{r^3 r'\gamma}{3}\int_{\varphi_1}^{\varphi_2} d\phi \quad \frac{\sin(\phi)^4}{B^2(\phi)D(\phi)}}_{\text{X}}.
\end{aligned}
\tag{37}
$$

The final integral X of eq. (37) can be expressed in form of elliptic integrals

$$
\begin{aligned}
X &= -\frac{r^3 r' \gamma}{3} \int_{\varphi_1}^{\varphi_2} d\phi \quad \frac{\sin(\phi)^4}{B^2(\phi) D(\phi)} \\
&= \frac{2r^3 r' \gamma}{3a} \int_{\alpha_1}^{\alpha_2} d\alpha \quad \frac{(4\sin(\alpha)^2 - 4\sin(\alpha)^4)^4}{B^2(\alpha)\sqrt{1 - k^2 \sin(\alpha)^2}} \\
&= \frac{2r^3 r' \gamma 4^4}{3a} \int_{\alpha_1}^{\alpha_2} d\alpha \quad \frac{\alpha_8 \sin(\alpha)^8 + \alpha_{10} \sin(\alpha)^{10}}{B^2(\alpha)\sqrt{1 - k^2 \sin(\alpha)^2}} \\
&\quad + \frac{\alpha_{12} \sin(\alpha)^{12} + \alpha_{14} \sin(\alpha)^{14} + \alpha_{16} \sin(\alpha)^{16}}{B^2(\alpha)\sqrt{1 - k^2 \sin(\alpha)^2}}
\end{aligned} \tag{38}
$$

which can be solved using the formulas provided in [33].

4) Integral I_4 of A_φ

For I_4, integration by parts yields

$$
\begin{aligned}
I_4 &= -r^2 \int_{\varphi_1}^{\varphi_2} d\phi \quad \sin(\phi)\cos(\phi)^2 \tan^{-1}\left(\beta_3(\phi)\right) \\
&= r^2 \frac{1}{3} \cos(\phi)^3 \tan^{-1}\left(\beta_3(\phi)\right)\Big|_{\phi=\varphi_1-\varphi}^{\phi=\varphi_2-\varphi} \\
&\quad + r^2 \frac{1}{3} \int_{\varphi_1}^{\varphi_2} d\phi \quad \cos(\phi)^3 \left[\frac{\gamma r(r - r'\cos(\phi))}{D(\phi)B^2(\phi)}\right. \\
&\quad + \left.\frac{\gamma r \cos(\phi)(r\cos(\phi) - r')}{D(\phi)G^2(\phi)}\right].
\end{aligned} \tag{39}
$$

The following integrals can be defined

$$
I_{41} = \frac{r^2}{3} \int_{\varphi_1}^{\varphi_2} d\phi \frac{\beta_3 \cos(\phi)^3 + \beta_4 \cos(\phi)^4}{D(\phi)B^2(\phi)} \tag{40}
$$

$$
I_{42} = \frac{r^2}{3} \int_{\varphi_1}^{\varphi_2} d\phi \frac{\beta_4' \cos(\phi)^4 + \beta_5' \cos(\phi)^5}{D(\phi)G^2(\phi)}. \tag{41}
$$

They can be transformed into elliptic integrals using transformation $\cos(\phi) = -(1 - 2\sin(\alpha)^2)$, yielding

$$
\begin{aligned}
I_{41} &= -\frac{2r^2}{3} \int_{\alpha_1}^{\alpha_2} d\alpha \frac{\alpha_0 + \alpha_2 \sin(\alpha)^2 + \alpha_4 \sin(\alpha)^4}{D(\alpha)B^2(\alpha)} \\
&\quad + \frac{\alpha_6 \sin(\alpha)^6 + \alpha_8 \sin(\alpha)^8}{D(\alpha)B^2(\alpha)}
\end{aligned} \tag{42}
$$

$$
\begin{aligned}
I_{42} &= -\frac{2r^2}{3} \int_{\alpha_1}^{\alpha_2} d\alpha \frac{\alpha_0 + \alpha_2 \sin(\alpha)^2 + \alpha_4 \sin(\alpha)^4}{D(\alpha)G^2(\alpha)} \\
&\quad + \frac{\alpha_6 \sin(\alpha)^6 + \alpha_8 \sin(\alpha)^8 + \alpha_{10} \sin(\alpha)^{10}}{D(\alpha)G^2(\alpha)}.
\end{aligned} \tag{43}
$$

B. Improved formulation of radial magnetic field (H_r)

Starting with the expression for H_r leads to

$$
H_r = H_{r1} + H_{r2} \tag{44}
$$

$$
H_{r1} = \int_{\varphi_1}^{\varphi_2} d\phi \quad \cos(\phi) D(\phi) \tag{45}
$$

$$
H_{r2} = \int_{\varphi_1}^{\varphi_2} d\phi \quad r\cos(\phi)^2 \sinh^{-1}\left(\beta_1(\phi)\right). \tag{46}
$$

The integration of the expression for H_{r1} is already done in the expression I_1 for A_ϕ. For the integration of H_{r2}, it is similar to the integration of I_2 for A_ϕ.

C. Improved formulation of angular magnetic field (H_φ)

The integration for H_φ is done in a similar way as for A_r. Integrating first over ϕ (integration by substitution), then over z' and finally over r', leads to

$$
\begin{aligned}
H_\varphi &= \int_{\varphi_1}^{\varphi_2} d\phi \int_{r_1}^{r_2} dr' \int_{z_1}^{z_2} dz' \frac{-\gamma r' \sin(\phi)}{D(\phi)^3} \\
&= \frac{1}{r} \int_{r_1}^{r_2} dr' \int_{z_1}^{z_2} dz' \frac{\gamma}{D(\phi)}\bigg|_{\phi=\varphi_1-\varphi}^{\phi=\varphi_2-\varphi} \\
&= \frac{1}{r} \int_{r_1}^{r_2} dr' D(\phi)\bigg|_{\phi=\varphi_1-\varphi}^{\phi=\varphi_2-\varphi}\bigg|_{z'=z_1}^{z'=z_2} \\
&= \frac{1}{r}\left((\gamma^2 + r^2 \sin(\phi)^2) \operatorname{arcsinh}\left(\frac{r' - r\cos(\phi)}{\sqrt{\gamma^2 + r^2 \sin(\phi)^2}}\right)\right. \\
&\quad + \left.\frac{1}{2}(r' - r\cos(\phi))D(\phi)\right)\bigg|_{r'=r_1}^{r'=r_2}\bigg|_{\phi=\varphi_1-\varphi}^{\phi=\varphi_2-\varphi}\bigg|_{z'=z_1}^{z'=z_2}.
\end{aligned} \tag{47}
$$

D. Improved formulation of axial magnetic field (H_z)

For H_z, the following integrals need to be calculated

$$
H_z = H_{z1} + H_{z2} + H_{z3} \tag{48}
$$

$$
H_{z1} = \int_{\varphi_1}^{\varphi_2} d\phi \quad \gamma \sinh^{-1}\left(\beta_1(\phi)\right) \tag{49}
$$

$$
H_{z2} = \int_{\varphi_1}^{\varphi_2} d\phi \quad -r\cos(\phi)\sinh^{-1}\left(\beta_2(\phi)\right) \tag{50}
$$

$$
H_{z3} = \int_{\varphi_1}^{\varphi_2} d\phi \quad -r\sin(\phi)\tan^{-1}\left(\beta_3(\phi)\right). \tag{51}
$$

As the first integral (H_{z1}) has no analytic expression, it will be evaluated numerically. For H_{z2}, using integration by parts leads to

$$
\begin{aligned}
H_{z2} &= \int_{\varphi_1}^{\varphi_2} d\phi \quad -r\cos(\phi)\sinh^{-1}\left(\beta_2(\phi)\right) \\
&= -r\sin(\phi)\sinh^{-1}\left(\beta_2(\phi)\right)\Big|_{\phi=\varphi_1-\varphi}^{\phi=\varphi_2-\varphi} \\
&\quad \underbrace{-r^2 r' \gamma \int_{\varphi_1}^{\varphi_2} d\phi \quad \frac{\sin(\phi)}{B^2(\phi)D(\phi)}}_{Y}.
\end{aligned} \tag{52}
$$

The remaining integral Y of eq. (52) will be transformed into an elliptic integral

$$
\begin{aligned}
Y &= -r^2 r' \gamma \int_{\varphi_1}^{\varphi_2} d\phi \quad \frac{\sin(\phi)}{B^2(\phi)D(\phi)} \\
&= \frac{8\gamma r^2 r'}{(r+r')^2 a} \int_{\alpha_1}^{\alpha_2} d\alpha \quad \frac{\sin(\alpha)^2 - \sin(\alpha)^4}{(1 - n^2 \sin(\alpha)^2)\sqrt{1 - k^2 \sin(\alpha)^2}}.
\end{aligned}
\tag{53}
$$

These elliptic integrals can be solved using the formulas of [33]. Finally, for H_{z3}

$$
\begin{aligned}
H_{z3} &= \int_{\varphi_1}^{\varphi_2} d\phi \quad - r\sin(\phi)\tan^{-1}\left(\beta_3(\phi)\right) \\
&= r\cos(\phi)\tan^{-1}\left(\beta_3(\phi)\right)\Big|_{\phi=\varphi_1-\varphi}^{\phi=\varphi_2-\varphi} \\
&\quad + \gamma r^2 \int_{\varphi_1}^{\varphi_2} d\phi \quad \cos(\phi)\Big[\frac{r - r'\cos(\phi)}{D(\phi)B^2(\phi)} \\
&\quad + \frac{\cos(\phi)(r\cos(\phi) - r')}{D(\phi)G^2(\phi)}\Big].
\end{aligned}
\tag{54}
$$

The solution can be separated into three parts where

$$
H_{z3} = \underbrace{r\cos(\phi)\tan^{-1}\left(\beta_3(\phi)\right)\Big|_{\phi=\varphi_1-\varphi}^{\phi=\varphi_2-\varphi}}_{H_{z31}} + H_{z32} + H_{z33}
$$

The integral parts are transformed into elliptic integrals, yielding

$$
H_{z32} = \gamma r^2 \int_{\varphi_1}^{\varphi_2} d\phi \cos(\phi)\frac{r - r'\cos(\phi)}{D(\phi)B^2(\phi)}
\tag{55}
$$

$$
H_{z33} = \gamma r^2 \int_{\varphi_1}^{\varphi_2} d\phi \cos(\phi)\frac{\cos(\phi)(r\cos(\phi) - r')}{D(\phi)G^2(\phi)}.
\tag{56}
$$

The solution of H_{z32} yields

$$
\begin{aligned}
H_{z32} &= \frac{2r^2\gamma}{a(r+r')^2} \int_{\alpha_1}^{\alpha_2} d\alpha(1 - 2\sin(\alpha)^2) \\
&\quad \frac{r + r'(1 - 2\sin(\alpha)^2)}{(1 - n^2\sin(\alpha)^2)\sqrt{1 - k^2\sin(\alpha)^2}} \\
&= \frac{2r^2\gamma}{a(r+r')^2} \int_{\alpha_1}^{\alpha_2} d\alpha \frac{\alpha_0 + \alpha_2\sin(\alpha)^2 + \alpha_4\sin(\alpha)^4}{(1 - n^2\sin(\alpha)^2)\sqrt{1 - k^2\sin(\alpha)^2}}.
\end{aligned}
\tag{57}
$$

In fact, these elliptic integrals can be solved using the formulas of [33]. Regarding H_{z33}, the transformation into elliptic integrals leads to

$$
\begin{aligned}
H_{z33} &= -\frac{2r^2\gamma}{a} \int_{\alpha_1}^{\alpha_2} d\alpha(1 - 2\sin(\alpha)^2)^2 \frac{r(1 - 2\sin(\alpha)^2) + r'}{G^2(\alpha)\sqrt{1 - k^2\sin(\alpha)^2}} \\
&= -\frac{2r^2\gamma}{a} \int_{\alpha_1}^{\alpha_2} d\alpha \frac{\alpha_0 + \alpha_2\sin(\alpha)^2 + \alpha_4\sin(\alpha)^4}{G^2(\alpha)\sqrt{1 - k^2\sin(\alpha)^2}} \\
&\quad + \frac{\alpha_6\sin(\alpha)^6}{G^2(\alpha)\sqrt{1 - k^2\sin(\alpha)^2}}.
\end{aligned}
\tag{58}
$$

Accordingly, these elliptic integrals can also be solved from known methodology [33].

E. Numerical computation of the novel expressions

The numerical evaluation of the novel expression is based on the numerical computational algorithms developed by Fukushima to compute the Jacobi-elliptic functions. Table I gives an overview of the practical computation algorithms used in this paper.

TABLE I: Overview of the used algorithms to compute the elliptic integrals and Jacobi-elliptic functions in the developed expressions.

Parameter names (refs.)	References	Equations (this paper)
$E(m)^a, E(\phi, m)^b$	[6], [20]	(28),(31)
$F(m), F(m, \phi)^c$	[19], [21], [22]	(28),(31)
$sn(u), cn(u), dn(u)^d$	[6]	(31),(32),(35),(38), (42),(43),(53),(57),(58)
$\Pi(m, n^2), \Pi(\phi, m, n^2)^e$	[23], [24]	(31),(32),(35),(38), (42),(43),(53),(57),(58)

[a]m represents the elliptic modulus or parameter, where E is the complete, respectively incomplete elliptic integral of the first kind.
[b]ϕ represents the amplitude in the jargon of elliptic functions and corresponds to α used in this paper, where ϕ was applied to stay consistent with the agreed notation in the field of elliptic functions.
[c]F is the complete, respectively incomplete elliptic integral of the second kind.
[d]sn, cn and dn depicts the Jacobi elliptic functions.
[e]n represents the characteristic where Π is the complete, respectively incomplete elliptic integral of the third kind.

V. VALIDATION OF THE NOVEL FORMULATIONS

A suitable TEAM-problem was not identified for a coil geometry in air with relevant benchmark values for the $\vec{H}$-field and or $\vec{A}$-field. As a consequence, this paper follows a similar approach, as presented in [35]. The validation of the novel equations is carried out in two separate validation studies, i.e.,

1) the magnetic field ($\vec{H}$-field) and
2) the magnetic vector potential ($\vec{A}$-field).

In all the cases where the results are assessed against 3-D FE calculations where the normalized relative difference

$$
(\textit{Error factor}) = \left| \frac{(\textit{Analytic}) - (\textit{3-D FE})}{(\textit{3-D FE})} \right|,
\tag{59}
$$

is utilized as a performance measure. The 3-D FE simulations have been performed using an A-V formulation with a tetrahedron mesh of the second-order (in terms of the $\vec{H}$-field). We also performed comparative simulation using an H-ϕ formulation with a second-order tetrahedron $\vec{H}$-field mesh, which showed no significant discrepancy against the A-V formulation. We, therefore, concluded that the choice of the formulation

has no significant impact on the precision of the numerical results. The results displayed later on are based on a A-V formulation simulation, which are obtained with a converging solution. The mesh density is incrementally increased until the final value is settled for the 5 to 7 digits precision, whereas each simulation converged using the "classical" minimum residual energy criterion (i.e., Gibbs free energy). Note that the impact of edge or node elements were not significant. For the $\vec{B}$-field, it has been verified that the 3-D FE solution is locally divergence-free, whereas the analytical solution is divergence-free per construction and the Laplacian of the $\vec{A}$-field is constant [14]. As a result, the first validation criteria for the $\vec{H}$-field and the $\vec{A}$-field are fulfilled. This as a necessary condition, but not an entirely conclusive condition.

In Section V-A, the proposed $\vec{H}$-field calculation is compared with 3-D FE simulations. In addition, Section V-B compares performance of the proposed formulation with the results of Fontana ([15]). The $\vec{A}$-field is validated in Section V-C, where the novel formulation for A_ϕ is compared to a numerical integration approach along the $d\phi$-direction. Moreover, the formula for A_r was validated using a symbolic calculation software (in the Mathematica environment) and further cross-checked with manual integration. In fact, no 3-D FE calculation was performed due to the lack of computational power available in the laboratory.

A. Validation of the $\vec{H}$-field using 3-D FE simulations
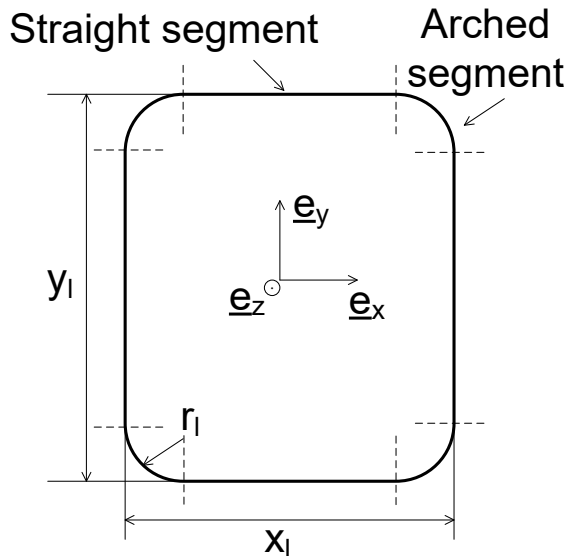

Fig. 2: Schematic representation of the round edges rectangular coil composed of 4 straight segments and 4 arched segments (refer to Fig. 1), the corresponding numerical values are given in Table II.

TABLE II: Specification of the simplified winding overhang (coil) geometry of a large electrical machine investigated.

Parameter	Description	Value	Unit
y_l	Length of coil rectangle	2800	mm
x_l	Width of coil rectangle	1550	mm
r_l	Edge radius of coil rectangle	150	mm
y	Height of coil cross-section	25	mm
x	Width of coil cross-section	10	mm
I_c	Total coil current	1	MA
B_c	Center-of-coil flux density	0.5	T

This subsection presents a case study of a large generic coil composed of four-arched current-carrying conductors (refer to Fig. 1) corresponding to the four corners of the coil represented in Fig. 2 and four straight conductors with analytic expression for the $\vec{H}$-field reported in [7]. The segments of the coil geometry represents elements of a simplified end-winding geometry of a large electrical machine, without any claim to represent a particular practical application of this geometry. The geometry considered is shown in Fig. 2 with specifications provided in Table II. Targeted validation paths are chosen and they are provided in the appendix Section VII-B (Fig. 7).
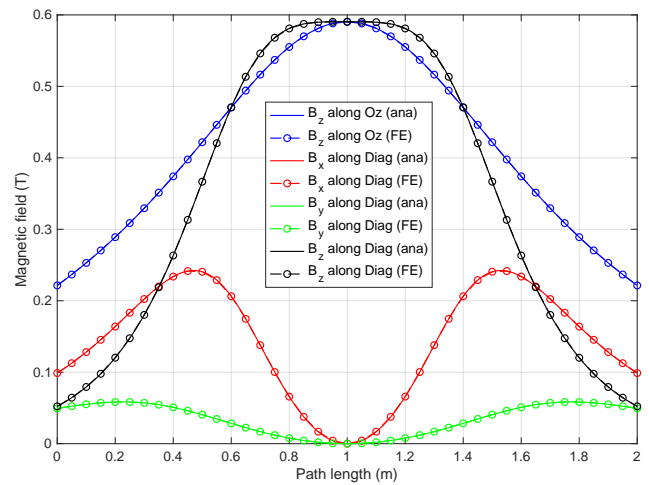

Fig. 3: $\vec{B}$-field (analytic calculation) along different paths, defined in Section VII-B and shown in Fig. 7 for the geometry defined in Fig. 2 using the numerical values given in Table II.

Analytical $\vec{B}$-field results (in Tesla) are shown in Fig. 3 along a couple of specified the paths. The field curves are assessed against 3-D FE results, which are in good agreement. Note that the $\vec{H}$-field and $\vec{B}$-field are related via the μ_0-constant in the given case. More evaluation paths are covered in Section VII-B.

The accuracy of the results in Fig. 3 are evaluated in Fig. 4 with respect to the final 3-D FE results. The absolute difference is shown to be very small over all of the evaluated paths, fluctuating between 10^{-6} T and 10^{-12} T, depending on the
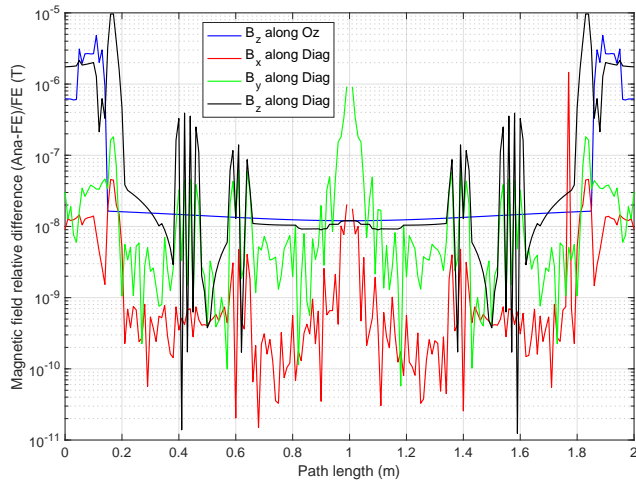
Fig. 4: Relative difference between the analytic and 3D-FE expressions and 3D-FE along different paths, defined in section -B and shown in Fig. 7 for the geometry defined in Fig. 2 using the numerical values given in Table II.

chosen path. The overall agreement demonstrates the significant precision of the proposed novel formulations. In general, it is not possible to draw conclusions from the error variation since the mesh density is not constant over the 3-D FE volume. However, it is worth noting that the error is generally reduced by at least one order of magnitude for B_x and B_y along *Diag* compared to B_z along *Diag*. The error is quasi-identical for B_z along *Oz* and *Diag* over a path length spanning from 0.2 to 1.8 m. The magnitude of the $\vec{B}$-field lies between $0.05\,\text{T}$ and $0.6\,\text{T}$ depending on the considered path. In general, the overall mean values highlighted in Table III support the already mentioned observations.

TABLE III: Comparison between the rectangular approximation against 3-D FE (rectangular cross-section) along different paths, defined in Section VII-B and shown in Fig. 7 for the geometry defined in Fig. 2 using the numerical values given in Table II.

Path	Rectangular approximation (T) mean value of the difference
B_z along Oz	7.8334e-08
B_x along Diag	1.7510e-09
B_y along Diag	6.9299e-10
B_z along Diag	5.4944e-08
B_x along OxOz+	1.4778e-09
B_z along OxOz+	7.9363e-08
B_z along OyOx-	7.9247e-08

Two normalized errors could be highlighted. Expressed in percentage, the mean value[1] becomes 3.0622e-05% for B_z

[1]Only two results could be presented as a percentage error since it converges toward 100% as the $\vec{B}$-field approaches toward zero.

along Oz and 5.4214e-05% for B_z along *Diag*. The normalized errors are very small, which demonstrates the excellent accuracy of the novel formulations for a scalable problem.

B. Benchmark of the $\vec{H}$-field formulaes with Fontana ([15])

From a previous study [15], the analytic expressions of [7] was compared with a numerical quadrature. However, this paper provides both novel expressions that are also assessed against 3-D FE results.

For the sake of fairness with respect to earlier studies, this case study selects 23 conventionally defined observation points (based on [15]) where the magnitude of the $\vec{H}$-field is computed. These points are shown in Fig. 5, and further specified in Table IV. In addition to the magnitude, the three components are also given in this table for both the 3-D FE results and the formulas proposed in this paper.
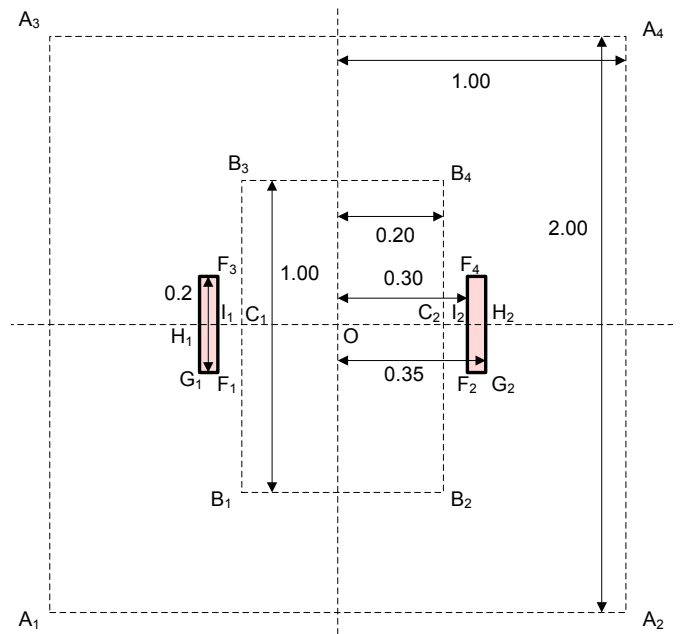

Fig. 5: Schematic representation (plane view of a cut) of the toroidal coil (highlighted in red) used in [15] and definition of the points Ai to Ii.

The $\vec{H}$-field magnitude is expected to be the same for all points A_i, B_i, C_i, F_i, G_i, H_i, I_i by the construction of the same geometry. In general, this is the case for both "Fontana, Urankar" and the analytic developments presented in this work for all points. However, the point F_i and G_i are located at a line singularity (bold values in Table IV). As a result, the error is significantly higher for these points due to their location. It is advised that the integral that computes these points should be carefully modified to take the singularity into account.

TABLE IV: Comparison of [15], 3-D FE computation and the proposed formulas (magnitude of $\vec{H}$-field expressed in A/m, results with 5 to 7 significant digits). Numerical values below 1e-15 have been written as 0.0, bolded values correspond to a line singularity.

Eval. point	$|\tilde{\mathbf{H}}|$				$\mathbf{H_x}$ [A/m]		$\mathbf{H_y}$ [A/m]		$\mathbf{H_z}$ [A/m]	
	Fontana, Fin. Vol. 39078	Fontana, Urankar	3-D FE	This work	3-D FE	This work	3-D FE	This work	3-D FE	This work
A_1	0.0147455	0.0147479	0.0147492	0.0147493	0.0138026	0.0138026	0.0	0.0	0.0051990	0.0051990
A_2	0.0147434	0.0147479	0.0147492	0.0147493	-0.0138026	-0.0138026	0.0	0.0	0.0051990	0.0051990
A_3	0.0147433	0.0147479	0.0147492	0.0147493	-0.0138026	-0.0138026	0.0	0.0	0.0051990	0.0051990
A_4	0.0147453	0.0147479	0.0147492	0.0147493	0.0138026	0.0138026	0.0	0.0	0.0051990	0.0051990
B_1	0.227051	0.227077	0.227066	0.227066	0.095322	0.095322	0.0	0.0	0.206089	0.206089
B_2	0.227041	0.227077	0.227066	0.227066	-0.095322	-0.095322	0.0	0.0	0.206089	0.206089
B_3	0.227033	0.227077	0.227066	0.227066	-0.095322	-0.095322	0.0	0.0	0.206089	0.206089
B_4	0.227038	0.227077	0.227066	0.227066	0.095322	0.095322	0.0	0.0	0.206089	0.206089
C_1	1.94055	1.9387	1.939178	1.939178	0.0	0.0	0.0	0.0	1.939178	1.939178
C_2	1.94027	1.9387	1.939178	1.939178	0.0	0.0	0.0	0.0	1.939178	1.939178
D	0.0294561	0.0294932	0.0294781	0.0294781	0.0	0.0	0.0	0.0	-0.0294781	-0.0294781
E	0.257634	0.257639	0.257642	0.257642	0.0	0.0	0.0	0.0	0.257642	0.257642
F_1	2.50891	2.56669	2.55683	2.56536	**1.82292**	**1.83486**	0.0	0.0	1.79286	1.79286
F_2	2.51103	2.56381	2.55683	2.56536	**-1.82292**	**-1.83486**	0.0	0.0	1.79286	1.79286
F_3	2.50699	2.56669	2.55683	2.56536	**-1.82292**	**-1.83486**	0.0	0.0	1.79286	1.79286
F_4	2.50811	2.56381	2.55683	2.56536	**1.82292**	**1.83486**	0.0	0.0	1.79286	1.79286
G_1	1.77891	1.82984	1.81714	1.82852	**1.72966**	**1.74162**	0.0	0.0	-0.55702	-0.55702
G_2	1.77643	1.82685	1.81714	1.82852	**-1.72966**	**-1.74162**	0.0	0.0	-0.55702	-0.55702
H_1	1.29946	1.34769	1.36403	1.36403	0.0	0.0	0.0	0.0	-1.36403	-1.36403
H_2	1.29565	1.34769	1.36403	1.36403	0.0	0.0	0.0	0.0	-1.36403	-1.36403
I_1	2.85931	2.94681	2.93738	2.93738	0.0	0.0	0.0	0.0	2.93738	2.93738
I_2	2.85431	2.94681	2.93738	2.93738	0.0	0.0	0.0	0.0	2.93738	2.93738
O	0.000000	0.000000	1.472740	1.472740	0.0	0.0	0.0	0.0	1.472740	1.472740

It should be highlighted that for all the observation points, the difference between our results and 3-D FE results is significantly lower than what is predicted by Fontana, confirming the excellent precision of the developed formulations.

The values generated from the finite volume method ("Fontana Fin. Vol.") and numerical evaluation of Urankar's equation ("Fontana, Urankar") have the biggest difference to the 3-D FE simulation. The magnitude is different for every point in the finite volume calculation, while there are 2 series of distinct values in the numerical evaluation of Urankar's equation. An increased number of volume elements will make the numerical values to reach the values of the 3-D FE simulation. One possible explanation is the fact that the numerical integration of Urankar's equation is not done with a sufficiently small integration steps, so that a relevant error is still present.

For point O, there seems to be a problem with the $\vec{H}$-field computed using "Fontana Fin. Vol. 39078" or "Fontana, Urankar" as they both show an amplitude of 0 [A/m], which is physically impossible, as the $\vec{H}$-field must have a non-zero component along the z-axis at the origin (as stated in [7]).

The last six columns of Table IV present a more detailed comparison between "This Work" and "3-D FE". The goal is to show which component of the $\vec{H}$-field is impacted by the line singularity. It is perceived that the x-component (or r-component in cylindrical coordinates) is the only component impacted by this singularity. As a result, possible corrections are to be considered for this component only.
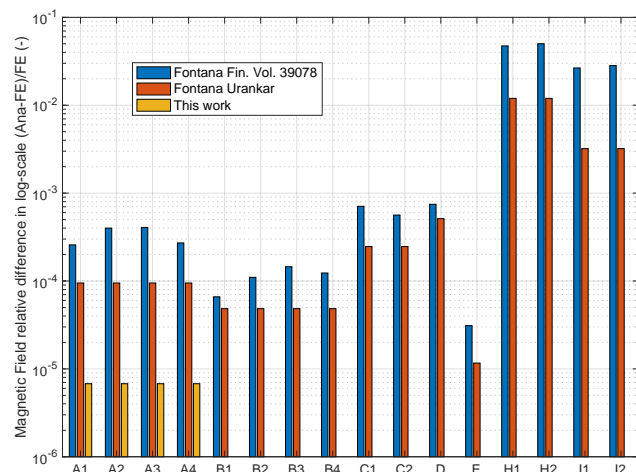

Fig. 6: Normalized relative difference of the $\vec{H}$-field for the points Ai to Ii (except line singularities) different computation methods compared to 3D-FE. The points Ai to Ii are defined in Fig. 5, results with 5 to 7 significant digits. The error of "This work" is equal to or less than 10^{-6} for points B_1, B_2, B_3, C_1, C_2, D, E, H_1, H_2, I_1 and I_2 in this figure.

Fig. 6 presents graphically the results of the first four columns of Table IV. The equations developed in this work

have no difference compared to the final FE values (with 5 to 7 significant digits), which demonstrates the significant gain in numerical precision of this analytical development. The error of the actual formulation lies between 0.1 and 5% depending on the considered point, while it is lower than 6.8e-4% for the novel formulation. It is perceived that the upper expectation in improvement is as high as four orders of magnitude (H1 and H2).

C. Validation of the $\vec{A}$-field using numerical integration

Finally, the analytic expressions for the $\vec{A}$-field in the tangential direction have been compared the results of numerical integration carried out in the MATLAB environment. Table V reveals a relative error of 4.625ϵ, where ϵ is the double-precision machine tolerance (i.e., 2.220446049250313e-16). Consequently, this finding confirms the effectiveness of the improved analytic expressions.

In fact, a contribution that numerically integrated Urankars' expressions [7] reported significant discrepancies with the numerical integration in this paper, as well as the novel analytic expressions. Unfortunately, it was not possible to follow the complete development of the benchmark expressions [7]. Therefore, it is not possible to detect possible errors in the benchmark expressions or possible errors in our the interpretation of the expressions [7].

TABLE V: Sample assessment of A_φ from finite arc segment using eq. (4) with an observer located at $(r, \varphi, z) = (1.345\,67\,\mathrm{m}, 0.457\,819\,410\,485\,735\,\mathrm{rad}, 0.123\,\mathrm{m})$ with an integration domain ranging from $\phi_1 = 0.179175501009738$ to $\phi_2 = 0.788860896633405$, from $r_1 = 0.5$ to $r_2 = 1.5$ and from $z_1 = 0$ to $z_2 = 1.0$.

	Value
Analytical evaluation	$0.152\,519\,106\,701\,134\,\mathrm{Wb/m}$
Numerical integration	$0.152\,519\,106\,701\,135\,\mathrm{Wb/m}$
Deviation	$< 5\epsilon$

VI. CONCLUSION

This paper demonstrates the utility of an improved 3-D integral magnetic field computation method of the $\vec{H}$-field and the $\vec{A}$-field. In our case study, we show the superiority of the proposed analytic formulations in comparison with alternative approaches ([7] - [12]). Moreover, it has been validated and assessed in a commercial 3-D FE environment. As a general rule of thumb, it must be highlighted that the novel expressions for the $\vec{H}$-field reduce the error on average by more than three orders of magnitude compared to the existing literature (Fig. 6). In addition, the expressions for the $\vec{A}$-field have been validated against numerical integration, and they present an error below ten times machine precision. The numerical

speed-up is achieved utilizing the algorithms developed by Fukushima.

Combining both advancements, i.e., the novel equations and Fukushima's algorithms, this work enables enhanced formulations of the analytic equations. In fact, they deploy their biggest advantage compared to the 3-D FE method, namely the fact that the individual contributions of each current-carrying segment can be easily identified. As a result, this work provides huge advantages in dealing with complex electromagnetic optimization problems. Moreover, the "on-demand" calculation provides the field quantities only at the needed locations, thus reducing the computational needs in obtaining any given result.

In a future research effort, the contribution of each current-carrying segment will be further investigated and the work will take into account the numerical error induced by the singularities.

VII. APPENDIX

A. Case of $r = 0$

In the case $r = 0$ the formulas for the $\vec{A}$-field and the $\vec{H}$-field gets

$$
\begin{aligned}
A_r &= \int_{\varphi_1}^{\varphi_2} d\phi \int_{r_1}^{r_2} dr' \int_{z_1}^{z_2} dz' \; \frac{-r'\sin(\phi)}{(\gamma^2 + r'^2)^{1/2}} \\
&= \cos(\phi) \int_{z_1}^{z_2} dz' \quad \sqrt{\gamma^2 + r'^2} \\
&= \frac{1}{2}\cos(\phi)\left(r'^2 \operatorname{arcsinh}\left(\frac{\gamma}{|r'|}\right) + \gamma\sqrt{\gamma^2 + r'^2} \right)\Bigg|_{r'=r_1}^{r'=r_2}\Bigg|_{\phi=\varphi_1-\varphi}^{\phi=\varphi_2-\varphi}\Bigg|_{z'=z_1}^{z'=z_2}
\end{aligned}
\tag{60}
$$

$$
\begin{aligned}
A_\varphi &= \int_{\varphi_1}^{\varphi_2} d\phi \int_{r_1}^{r_2} dr' \int_{z_1}^{z_2} dz' \; \frac{r'\cos(\phi)}{(\gamma^2 + r'^2)^{1/2}} \\
&= \sin(\phi) \int_{z_1}^{z_2} dz' \quad \sqrt{\gamma^2 + r'^2} \\
&= \frac{1}{2}\sin(\phi)\left(r'^2 \operatorname{arcsinh}\left(\frac{\gamma}{|r'|}\right) + \gamma\sqrt{\gamma^2 + r'^2} \right)\Bigg|_{r'=r_1}^{r'=r_2}\Bigg|_{\phi=\varphi_1-\varphi}^{\phi=\varphi_2-\varphi}\Bigg|_{z'=z_1}^{z'=z_2}
\end{aligned}
\tag{61}
$$

$$
\begin{aligned}
H_r &= \int_{\varphi_1}^{\varphi_2} d\phi \int_{r_1}^{r_2} dr' \int_{z_1}^{z_2} dz' \; \frac{-\gamma r'\cos(\phi)}{(\gamma^2 + r'^2)^{3/2}} \\
&= \sin(\phi) \int_{z_1}^{z_2} dz' \quad \frac{\gamma}{\sqrt{\gamma^2 + r'^2}} \\
&= \sin(\phi)\sqrt{\gamma^2 + r'^2}\,\Bigg|_{r'=r_1}^{r'=r_2}\Bigg|_{\phi=\varphi_1-\varphi}^{\phi=\varphi_2-\varphi}\Bigg|_{z'=z_1}^{z'=z_2}
\end{aligned}
\tag{62}
$$

$$H_\varphi = \int_{\varphi_1}^{\varphi_2} d\phi \int_{r_1}^{r_2} dr' \int_{z_1}^{z_2} dz' \; \frac{-\gamma r' \sin(\phi)}{(\gamma^2 + r'^2)^{3/2}}$$

$$= -\cos(\phi) \int_{z_1}^{z_2} dz' \; \frac{\gamma}{\sqrt{\gamma^2 + r'^2}}$$

$$= -\cos(\phi)\sqrt{\gamma^2 + r'^2} \Big|_{r'=r_1}^{r'=r_2} \Big|_{\phi=\varphi_1-\varphi}^{\phi=\varphi_2-\varphi} \Big|_{z'=z_1}^{z'=z_2} \quad (63)$$

$$H_z = \int_{\varphi_1}^{\varphi_2} d\phi \int_{r_1}^{r_2} dr' \int_{z_1}^{z_2} dz' \; \frac{r'^2}{(\gamma^2 + r'^2)^{3/2}}$$

$$= \phi \int_{z_1}^{z_2} dz' \quad \operatorname{arcsinh}(\frac{r'}{|\gamma|}) - \frac{r'}{\sqrt{\gamma^2 + r'^2}} \Big|_{r'=r_1}^{r'=r_2}$$

$$= \phi\gamma \left(\operatorname{arcsinh}(\frac{r'}{|\gamma|}) - 1 \right) \Big|_{r'=r_1}^{r'=r_2} \Big|_{\phi=\varphi_1-\varphi}^{\phi=\varphi_2-\varphi} \Big|_{z'=z_1}^{z'=z_2} \quad (64)$$

B. Validation paths

$$\text{Ox} = \begin{cases} t & \text{with } t \in [-2, 2], \text{ 400 samples} \\ 0 \\ 0 \end{cases} \quad (65)$$

$$\text{OxD} = \begin{cases} t & \text{with } t \in [0.6, 1], \text{ 600 samples} \\ 0 \\ 0 \end{cases} \quad (66)$$

$$\text{OxOy+} = \begin{cases} t & \text{with } t \in [-2, 2], \text{ 400 samples} \\ 1.75 \\ 0 \end{cases} \quad (67)$$

$$\text{OxOz+} = \begin{cases} t & \text{with } t \in [-2, 2], \text{ 400 samples} \\ 0 \\ 1.25 \end{cases} \quad (68)$$

$$\text{Oy} = \begin{cases} 0 \\ t & \text{with } t \in [-2, 2], \text{ 400 samples} \\ 0 \end{cases} \quad (69)$$

$$\text{OyOx-} = \begin{cases} -1.75 \\ t & \text{with } t \in [-2, 2], \text{ 400 samples} \\ 0 \end{cases} \quad (70)$$

$$\text{Oz} = \begin{cases} 0 \\ 0 \\ t & \text{with } t \in [-1, 1], \text{ 200 samples} \end{cases} \quad (71)$$

$$\text{Oz-Ox+Oy} = \begin{cases} -0.5 \\ 0.5 \\ t & \text{with } t \in [-1, 1], \text{ 200 samples} \end{cases} \quad (72)$$

$$\text{Oz+Ox+Oy} = \begin{cases} 0.5 \\ 0.5 \\ t & \text{with } t \in [-1, 1], \text{ 200 samples} \end{cases} \quad (73)$$

$$\text{Diag} = \begin{cases} t & \text{with } t \in [-1, 1], \text{ 200 samples} \\ t & \text{idem} \\ t & \text{idem} \end{cases} \quad (74)$$
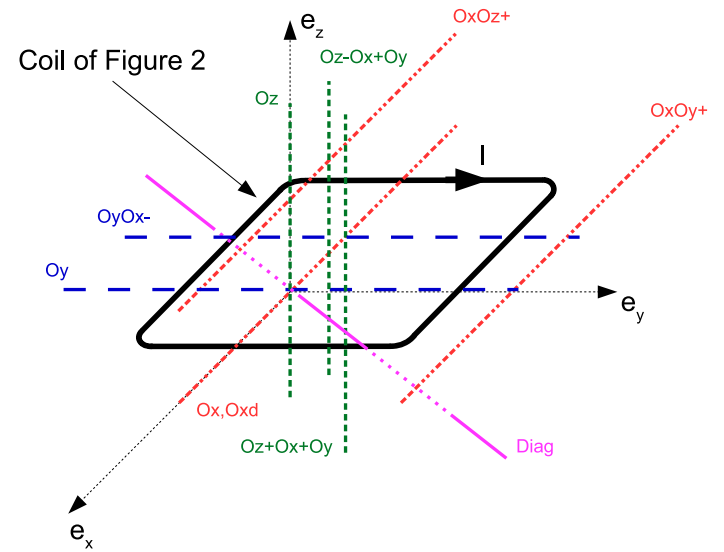
The validation paths are depicted in figure 7.

Fig. 7: Schematic representation of the validation paths used to validate the novel expressions.

REFERENCES

[1] C. Niu, X. Zhu, Q. Wang, Y. Li, F. Tang and F. Liu. A Novel Design Method of Independent Zonal Superconducting Shim Coil. *IEEE Trans. Appl. Superconduct.*, 29(1):1–8, Jan 2019.
[2] S. Liang and Y. Fang. Analysis of Inductance Calculation of Coaxial Circular Coils With Rectangular Cross Section Using Inverse Hyperbolic Functions. *IEEE Trans. Appl. Superconduct.*, 25(4):1–9, Aug 2015.
[3] S. Babic and C. Akyel. Calculation of Some Electromagnetic Quantities for Circular Thick Coil of Rectangular Cross-Section and Pancake with Inverse Radial Currents. *IET Elect. Power Appl.*, 12(9):1306–1310, Nov 2018.
[4] S. Babic and C. Akyel. Mutual Inductance and Magnetic Force Calculations between Thick Bitter Circular Coil of Rectangular Cross Section with Inverse Radial Current and Filamentary Circular Coil with Constant Azimuthal Current. *IET Elect. Power Appl.*, 11(9):1596–1600, Nov 2017.
[5] T. Kang, T. Chen, Y. Wang and K.I. Kim. A T-ψ formulation with the penalty function term for the 3D eddy current problem in laminated structures. *Appl. Math. Comp.*, 271:618–641, Nov 2015.

[6] T. Fukushima. Fast computation of complete elliptic integrals and Jacobian elliptic functions. *Cel. Mech. Dyn. Astron.*, 105(4):305–328, Dec 2009.

[7] L. Urankar. Vector potential and magnetic field of current-carrying finite arc segment in analytical form, Part III: Exact computation for rectangular cross section. *IEEE Trans. Magn.*, 18(6):1860–1867, Nov 1982.

[8] L. Urankar. Vector potential and magnetic field of current-carying finite arc segment in analytical form, Part I: Filament approximation. *IEEE Trans. Magn.*, 16(5):1283–1288, Sept 1980.

[9] L. Urankar. Vector potential and magnetic field of current-carying finite arc segment in analytical form, part II: Thin sheet approximation. *IEEE Trans. Magn.*, 18(3):911–917, May 1982.

[10] L. Urankar. Vector potential and magnetic field of current-carying finite arc segment in analytical form, part IV: General three-dimensional current density. *IEEE Trans. Magn.*, 20(6):2145–2150, Nov 1984.

[11] L. Urankar. Common compact analytical formulas for computation of geometry integrals on a basic conic sub-domain in boundary and volume integral methods. *Eng. Analysis with Boundary Elem.*, 7(3):124–129, 1990.

[12] L. Urankar. Common compact analytical formulas for computation of geometry integrals on a basic conic sub-domain in boundary and volume integral methods. *Archiv für Elektrotechnik*, 73:97–107, 1990.

[13] V. I. Danilov and M. Ianovici. Magnetic Field of DC Coils of Cyélindrical Configuration. *Nuclear Instr. Meth.*, 79:29–42, 1970.

[14] V. I. Danilov and M. Ianovici. Magnetic field of thick finite dc solenoids. *Nuclear Instr. Meth.*, 94(3):541–550, 1971.

[15] M. Fontana. Integration methods for the calculation of the magnetostatic field due to coils, 2001.

[16] Y. Yang, H. Xia, G. Ni and X. Liang. 3-D eddy current analysis in the end region of a turbogenerator by using reduced magnetic vector potential. *IEEE Trans. Magn.*, 42(4):1323-1326, Apr 2006.

[17] L. Urankar and P. Henninger. Compact Extended Algorithms for Elliptic Integrals in Electromagnetic Field and Potential Computations Part I: Elliptic Integrals of the First and Second Kind with Extended Integration Range. *IEEE Trans. Magn.*, 27(5):4338–4342, Sept 1991.

[18] L. Urankar, P. Henninger and F.S. Nestel. Compact Extended Algorithms for Elliptic Integrals in Electromagnetic Field and Potential Computations Part II: Elliptic Integral of the thirs Kind with Extended Integration Range. *IEEE Trans. Magn.*, 30(3):1236–1241, May 1994.

[19] T. Fukushima. Fast computation of Jacobian elliptic functions and incomplete elliptic integrals for constant values of elliptic parameter and elliptic characteristic. *Cel. Mech. Dyn. Astron.*, 105(1-3):245–260, Nov 2009.

[20] T. Fukushima. Fast computation of incomplete elliptic integral of first kind by half argument transformation. *Numerische Mathematik*, 116(4):687–719, Oct 2010.

[21] T. Fukushima. Precise and fast computation of a general incomplete elliptic integral of second kind by half and double argument transformations. *J. Comp. Appl. Mathematics*, 235(14):4140–4148, May 2011.

[22] T. Fukushima. Precise and fast computation of the general complete elliptic integral of the second kind. *Mathematics of Computation*, 80(275):1725–1743, 2011.

[23] T. Fukushima. Precise and fast computation of a general incomplete elliptic integral of third kind by half and double argument transformations. *J. Comp. Appl. Mathematics*, 236(7):1961–1975, Jan 2012.

[24] T. Fukushima. Fast computation of a general coplete elliptic integral of the third kind by half and double argument transformation. *J. Comp. and Appl. Mathematics*, 253:142–157, 2013.

[25] Y. Zhao, B. Yan, C. Zeng, S. Huang, C. Chen and J. Deng. Optimal Scheme for Structural Design of Large Turbogenerator Stator End Winding. *IEEE Trans. Energy Convers.*, vol. 31, no. 4, pp. 1423–1432, 2016.

[26] R.D. Stancheva and I.I. Iatcheva. Compact 3-D Electromagnetic Force Distribution in the End Region of Turbogenerator. *IEEE Trans. Magn.*, vol. 45, no. 3, pp. 1000–1003, 2009.

[27] K.C. Kim, H.W. Lee, Y.D. Chun and J. Lee. Compact Analysis of Electromagnetic Force Distribution on End Winding for Motor Reliance. *IEEE Trans. Magn.*, vol. 41, no. 10, pp. 4072–4074, 2005.

[28] E. Rochepault, P. Vedrine and F. Bouillault. Compact 2D Analytical Magnetic Optimizations for Accelerator Dipole Block Designs. *IEEE Trans. Appl. Superconduct.*, vol. 22, no. 3, pp. 4900804?4900804, 2012.

[29] E. Rochepault, P. Vedrine, G. Aubert and F. Bouillault. Compact 3D magnetic optimization of dipole ends with rectangular cross-sections. *Europ. Physical J. Appl. Physics*, vol. 64, no. 2, p. 24507, Nov 2013.

[30] S.I. Babic and C. Akyel. Compact New Analytic-Numerical Solutions for theMutual Inductance of Two Coaxial Circular CoilsWith Rectangular Cross Section in Air. *IEEE Trans. Magn.*, 42(6):1661-1669, Jun 2006.

[31] S.I. Babic, C. Akyel, Y. Ren and W. Chen. Compact Magnetic force calculation between circular coils of rectangular cross section with parallel axes for superconducting magnet. *Progr. Electromagn. Research B*, vol. 37, pp. 275-288, 2012.

[32] J.T. Conway. Compact Inductance Calculations for Circular Coils of Rectangular Cross Section and Parallel Axes Using Bessel and Struve Functions. *IEEE Trans. Magn.*, vol. 46, no. 1, pp. 75-81, Jan 2010.

[33] P.F. Byrd and M.D. Friedman. *Handbook of Elliptic Integrals for Engineers and Scientists*. Springer-Verlag Berlin Heidelberg New York, second edition, revised edition, 1971.

[34] W. Bartky. *Numerical Calculation of a Generalized Complete Elliptic Integral*. American Physical Society, vol. 10, iss. 4, pp. 264–269, 1938.

[35] R. Ravaud, G. Lemarquand, V. Lemarquand and C. Depollier. Analytical Calculation of the Magnetic Field Created by Permanent-Magnet Rings. *IEEE Trans. Magn.*, 44(8):1982–1989, Aug 2008.

APPENDIX A
BIOGRAPHIES

Frederic Maurer received his master degree in 2009 and the Ph.D. degree in 2019 from the Swiss Federal Institute of Technology in Lausanne (EPFL). Since april 2009, he is working for Alstom Hydro (now GE Hydro) in different position: R&D engineer in the generator technology center, Lead electrical engineer and technical project manager.

Basile Kawkabani (M'00-SM'11) received the master's degree from Ecole Superieure d'Electricite (SUPELEC), Paris, France, in 1978, and the Ph.D. degree in electrical engineering from the Ecole Polytechnique Federale de Lausanne (EPFL), Lausanne, Switzerland, in 1984. From 1992 to 2010, he was a Lecturer and Research Associate in electrical machines at the Electrical Machinery Laboratory, EPFL and till April 2017 a Senior Scientist at EPFL.

Jonas Kristiansen Nøland (S'14-M'17) received the Ph.D. degree in engineering physics from Uppsala University, Uppsala, Sweden, in 2017. He is currently an Associate Professor with the Department of Electric Power Engineering, Norwegian University of Science and Technology, Trondheim, Norway. His research interests include excitation systems, salient-pole synchronous generators, and their interplay with the power system. August 2019, Dr. Nøland was appointed to serve as an Editor for the IEEE TRANSACTIONS ON ENERGY CONVERSION.